Optimising production of a biochar made from conifer brash and investigation of its potential for phosphate and ammonia removal

Industrial Crops & Products 185 (2022) 115165

Contents lists available at ScienceDirect

Industrial Crops & Products

journal homepage: www.elsevier.com/locate/indcrop

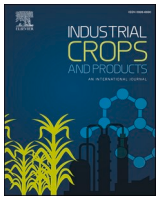

Optimising production of a biochar made from conifer brash and investigation of its potential for phosphate and ammonia removal

Sabolc Pap [a,b,*,1], Paul P.J. Gaffney [a], Qunying Zhao [a,c], Daniela Klein [d], Yuan Li [a,e], Caroline Kirk [f], Mark A. Taggart [a]

[a] Environmental Research Institute, UHI North Highland, University of the Highlands and Islands, Thurso, Caithness, Scotland, KW14 7JD, UK
[b] University of Novi Sad, Faculty of Technical Sciences, Department of Environmental Engineering and Occupational Safety and Health, Trg Dositeja Obradovića 6, 21 000, Novi Sad, Serbia
[c] School of Civil & Architecture Engineering, Xi'an Technological University, Xi'an, Shaan Xi, 710021,China
[d] RSPB Forsinard Flows, Flows Field Centre, Forsinard, Sutherland, Scotland, KW13 6YT, UK
[e] Environmental Development Center, Ministry of Ecology and Environment, Beijing 100029, China
[f] School of Chemistry, University of Edinburgh, David Brewster Rd, Edinburgh EH9 3FJ, UK

ARTICLE INFO

Keywords:
Wood waste
Circular economy
Nutrients
Water treatment
Peatland restoration
Central composite design

ABSTRACT

As a lignocellulose biomass, waste conifer brash (waste treetops and branches) from felled afforested peatland sites can be converted to biochar through pyrolysis, thus creating a potentially useful product. Here, we propose that brash from 'forest-to-bog' peatland restoration sites through conversion to biochar, could be utilised for nutrient (PO_4^{3-}-P and NH_4^+-N) removal at such restoration sites, or within the water sector. As a first step, we explore the factors involved in biochar production that will result in high nutrient adsorption efficiency and pyrolysis yield and low production cost (using a Plackett-Burman experimental design (PBD)). Central composite design (CCD) was used for further optimisation of pyrolysis time and temperature as the two most significant factors. Model predictions for an optimised biochar (OB) suggested pyrolysis conditions of 500 °C for 30 min could achieve the highest yield of 34.75 %, the lowest cost of 0.37 £ /kg, and the highest PO_4^{3-}-P and NH_4^+-N removal of 9.9 % and 65.2 %, respectively. Additionally, the OB morphology, structure and surface chemistry were characterised using different instrumental techniques which showed typical features for a wood-based biochar. While the OB did remove NH_4^+-N from solution (due to the presence of negatively charged functional groups), it did not remove significant amounts of PO_4^{3-}-P, indeed it leached PO_4^{3-}-P back into solution. Therefore, an unmodified biochar produced from conifer brash did not fulfil the aim of removing these two key nutrient pollutants for use in improving water quality at restoration sites. To address this challenge, the surface chemistry of the OB could be functionalised to increase its affinity toward both PO_4^{3-}-P and NH_4^+-N ions.

1. Introduction

Across Europe and beyond, restoration of previously afforested peatlands (through tree removal) is a growing practice aiming to improve the ecosystem services provided by peatland areas, including biodiversity conservation, water provision, atmospheric carbon sequestration and thus climate regulation (Bonn et al., 2016). This practice emerged in blanket bog peatlands, following increased awareness of the negative impacts of drainage and conifer plantations on blanket bog vegetation, breeding waders, peatland carbon stocks and surface water quality (Anderson et al., 2016; Wilson et al., 2014). While restoration of drained afforested blanket bogs (termed 'forest-to-bog' restoration) can re-instate key ecosystem services over a long time frame, i.e., after around 20 years post-felling (Gaffney et al., 2018; Hambley et al., 2019; Hancock et al., 2018), certain short term (potentially negative) effects of restoration can occur related to peatland ecohydrology and biogeochemical processes (Gaffney et al., 2021, 2018). One of these effects is altered pore- and surface-water chemistry following restoration, attributed (in part) to decomposition of brash – the treetops and branches which can remain on site and decompose post-restoration; and, the rewetting of previously aerobic peat (Gaffney et al., 2021, 2018; Shah and Nisbet, 2019). The main water chemistry

* Correspondence to: Environmental Research Institute, UHI North Highland, University of the Highlands and Islands, Thurso, Scotland, KW14 7JD, UK.
E-mail addresses: szabolcs.pap@uhi.ac.uk, sabolcpap@uns.ac.rs (S. Pap).
[1] ORCID: 0000-0001-7395-1913

https://doi.org/10.1016/j.indcrop.2022.115165
Received 2 March 2022; Received in revised form 13 May 2022; Accepted 28 May 2022
Available online 4 June 2022

changes associated with restoration are commonly increased concentrations of nutrients (ammonium-nitrogen; NH_4^+-N and phosphate; PO_4^{3-}-P) in run-off, which may be detected locally in streams and may also reach main rivers, depending on the proportion of the catchment undergoing restoration. While elevated NH_4^+-N and PO_4^{3-}-P can have negative impacts on downstream ecology and this is monitored in major rivers under the EU Water Framework Directive, there are also more localised impacts. For example, elevated pore-water nutrient concentrations can encourage vascular plant growth and retard the recovery of native blanket bog vegetation, particularly sphagnum mosses (Bubier et al., 2007; Hancock et al., 2018), which are the main peat forming vegetation in blanket bogs.

One way in which elevated nutrient concentrations following restoration can be reduced is by removing brash from restoration areas. However, this involves significant extra costs and extra passes of machinery on peatland restoration sites, although it is thought that (in the longer-term) brash removal is beneficial to both water quality and the restoration process. Once removed, there is currently limited use for brash, which is essentially a waste product. Some wood pellet producers may collect brash for pellet production, but this largely depends on the volume and quality of brash as well its accessibility to harvesting machinery. Thus, the cost of brash removal may often be prohibitive. As a lignocellulose biomass, brash can alternatively be converted to a biochar through pyrolysis (high temperature, low oxygen decomposition) (Gao et al., 2022; Mood et al., 2021; Vu and Do, 2021). Biochar derived from lignocellulose material has been effectively used for many purposes previously, including water treatment (e.g., removal of metals, nutrients) (Cheng et al., 2021b; Oginni and Singh, 2021; Rana et al., 2021), leachate treatment (Pap et al., 2021a, 2021b) and in soil amendment to improve soil physical and chemical properties (Fatima et al., 2021; Guo et al., 2021; Rana et al., 2022). Here, we propose that brash from forest-to-bog restoration sites may be converted to biochar, thus creating an added-value product marketable for water treatment, which could offset some of the costs of brash removal in restoration. Alternatively, biochar could itself be used on-site, to help reduce nutrient concentrations (NH_4^+-N and PO_4^{3-}-P) in surface water run-off following peatland restoration and/or conventional forestry felling operations.

Thus, the aim of this work was to investigate the potential for production and use of biochar derived from conifer brash in water treatment. Specifically, we aimed to determine the best production methods for biochar using conifer brash including variables such as: brash type (conifer species), pre-treatment, granulation, pyrolysis time and temperature. We also evaluated nutrient removal efficiency (NH_4^+-N and PO_4^{3-}P) for the biochars produced, characterised the optimum biochar and make future recommendations for producing biochar suitable for nutrient removal, including certain economic considerations.

2. Material and methods

2.1. Brash collection and preparation

Conifer brash (tree branches and tops) was collected from Forsinard Flows National Nature Reserve (NNR; - 58.357, - 3.897; latitude/longitude) in northern Scotland, managed by the Royal Society for the Protection of Birds (RSPB). Here, large areas of blanket bog peatland were drained and afforested with non-native conifers (Sitka spruce (*Picea sitchensis*) and lodgepole pine (*Pinus contorta*)) during the 1970 s to early 1990 s. Since acquiring the reserve and adjacent forestry plantations, the RSPB have been undertaking a programme of forest-to-bog restoration (starting in 1998 on older plantations), which is ongoing and has gathered pace in recent years.

Brash from both Sitka spruce and Lodgepole pine was collected from a recent forest-to-bog restoration area in November 2020. Here, trees were felled approximately two months prior to brash collection. The main tree stems were harvested while brash remained on site. Both tree species were intermixed and thus brash from each was available for collection. Large pieces of brash were cut to approximately $\leq$ 50 cm using loppers to fit into collection boxes. On return to the laboratory, brash was then cut into small pieces (~5 cm) using gardening secateurs for biochar production. Approximately half of the brash was then oven dried. Half of the dried brash (along with half of the undried brash) was then milled into ~0.1–1 mm powder with a mechanical mill (Retsch ZM 100), as part of the biochar synthesis optimisation process (see Sections 2.4–2.6). Pyrolysis was subsequently carried out in a muffle furnace (Carbolite CWF 1200). After cooling, biochars were washed with Milli-Q water to remove colour and ash, dried at 105 °C overnight, and stored in plastic bags for further use.

2.2. Chemicals and reagents

Ammonium chloride (NH_4Cl) and potassium dihydrogen phosphate (KH_2PO_4) were purchased from Fisher Chemicals UK. These reagents were of analytical grade and used without further purification. NH_4^+-N and PO_4^{3-}-P stock solutions (1000 mg/L) were prepared in Milli-Q water.

2.3. Instrumentation and characterisation

Water samples were analysed for nutrient concentrations using a Seal AQ2 discrete analyser. The concentration of P was measured as phosphate (PO_4^{3-}-P) using the ascorbic acid method while N was measured as ammonium (NH_4^+-N), using a variation of the indophenol green method (APHA, 2005). Absorbance readings were performed at 880 nm for PO_4^{3-}-P and at 670 nm for NH_4^+-N (Seal Analytical, UK).

The yield of biochar is an indication of the pyrolysis process mass efficiency (Bursztyn Fuentes et al., 2020). The following equation was used to calculate the yield of biochar:

$$Yield \quad (\%) = \frac{w_0 - w_p}{w_0} \times 100 \tag{1}$$

where: w_0 is the mass of biomass before pyrolysis and w_p is the mass of biochar.

The optimised biochar (OB) was tested using proximate analysis, and for point of zero charge (pH_{pzc}), suspension pH (pH_{sus}) and bulk density. Fourier transform infrared (FTIR) spectroscopy (Perkin Elmer Spectrum) was used to determine the functional groups present in the biomass and optimised biochar at a resolution of 1 cm^{-1} from 4000 to 500 cm^{-1}. Low-temperature (77 K) N_2 adsorption/desorption isotherms were obtained with a Quantachrome Quadrasorb evo surface area analyser. Powdered samples were degassed for 24 h at 105 °C under a high vacuum prior to analysis. An X-ray diffractometer (XRD) (D2 Phaser diffractometer, Bruker, Germany) was employed to analyse the mineralogical characteristics of the biochar at the 2 θ angles in the 6–60° range with Cu Kα radiation at a voltage of 40 kV, with a step size of 0.02°. A JEOL JSM-7800-F Field Emission Scanning Electron Microscope (FE-SEM) was used for morphology analysis at an accelerating voltage of 20 kV and approximate beam current of 1 nA. An Oxford Instruments X-max 80 mm^2 detector was used for Energy dispersive X-ray spectroscopy (EDX) analysis, combined with the AzTec software to quantify elemental composition at the biochar surface. XPS was performed on a Thermo K Alpha using an Al Kα mono-chromated (1486.6 eV) source with an overall energy resolution of ≈ 350 meV. The analysis area captured was approximately 400 μm x 600 μm, and this was carried out in the centre of the sample to check for the elements present.

2.4. Adsorption experiments

Bench adsorption trials were used to optimise the biochar synthesis process conditions regarding PO_4^{3-}-P and NH_4^+-N removal. Known masses (250 mg) of each biochar produced were thoroughly mixed with 20 mL of 20 mg/L PO_4^{3-}-P or NH_4^+-N solution. The pH of solutions was measured (using a Jennway 3520 pH meter), before and after adsorption

Table 1
Experimental ranges and levels for the factors used in the Plackett–Burman experimental design.

Factors	Levels		
	Low (−1)	Central (0)	High (+1)
A - Brash type	Lodgepole Pine	Mix	Sitka Spruce
B - Pre-treatment	No drying	Mix	Dried
C - Granulation	Cut	Mix	Milled
D - Time (min)	30	75	120
E - Temperature (°C)	300	550	800

Table 2
Process parameters and their coded levels for the central composite design (CCD) experimental design.

Factors	Levels				
	Lowest (-α)	Low (−1)	Central (0)	High (+1)	Highest (+α)
A - Temperature (°C)	500	544	650	756	800
B - Time (min)	30	43	75	107	120

(no pH adjustment was applied). Suspensions were shaken at a fixed temperature (ambient lab temperature ≈20 °C) for 24 h with an orbital shaker (IKA KS 260 basic) at 200 rpm. After shaking, samples were filtered through 0.45 μm nylon syringe filters (Fisherbrand). All experiments were conducted in duplicate with control and blank samples and the reported results were mean ± standard deviation. The percentage of phosphate and ammonium removal, R (%), and the equilibrium adsorption capacity, q_e (mg/g), were calculated, respectively, from the equations given below:

$$R \quad (\%) = \frac{C_0 - C_e}{C_0} \times 100 \tag{2}$$

$$q_e = \frac{(C_0 - C_e)}{m} \times V \tag{3}$$

Where C_0 is the initial nutrient concentration and C_e is the residual nutrient concentration (mg/L), V is the volume of solution (mL) and m is the mass of the biochar (g).

2.5. Screening of significant factors using a Plackett–Burman experimental design

Screening designs (Plackett–Burman design (PBD)) were used to identify the most important production factors from a large number of factors (Suryawanshi et al., 2021). In the present study, the pyrolysis and adsorption processes (pyrolysis yield (Y_1), production cost (Y_2), adsorption efficiency for PO_4^{3-}-P (Y_3) or NH_4^+-N (Y_4)) were all studied based on the results obtained from the experimental design where brash type (A), pre-treatment (B), granulation (C), pyrolysis time (D) and temperature (E) were selected as variables in the process. The Plackett–Burman method designed experiments at two levels: − 1 for low level, + 1 for high level and 0 for the centre point (Table 1) where the five variables were assessed using 13 lab trials (conducted in duplicate, giving a total of 26) (Table S1). The order of experiments was randomised. The experimental design was built using Minitab software version 18.0 (Minitab Inc., Pennsylvania, USA).

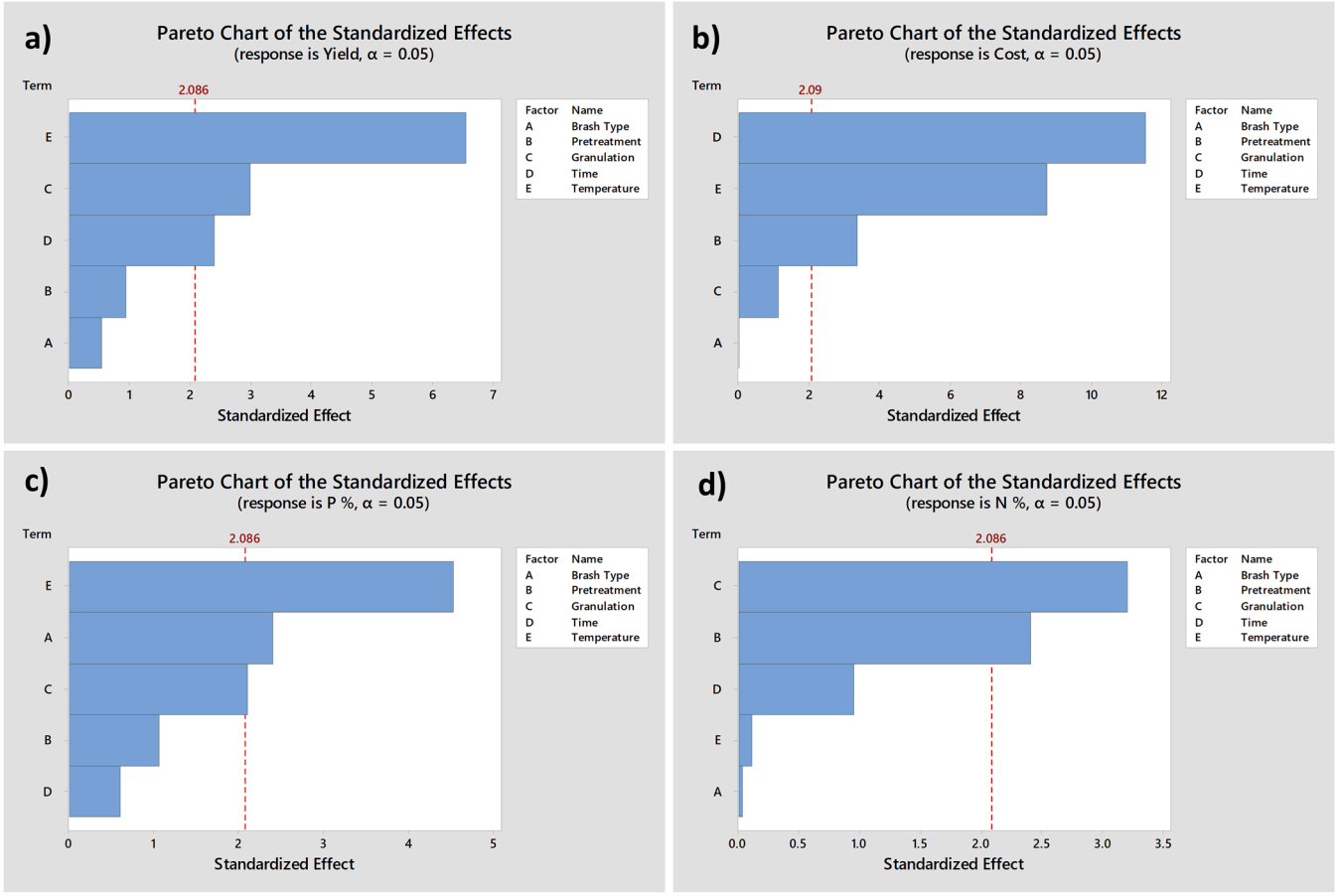

Fig. 1. Pareto chart of parameter effects from the screening analysis on pyrolysis yield (a), cost (b), PO_4^{3-}-P removal efficiency (c) and NH_4^+-N removal efficiency (d).

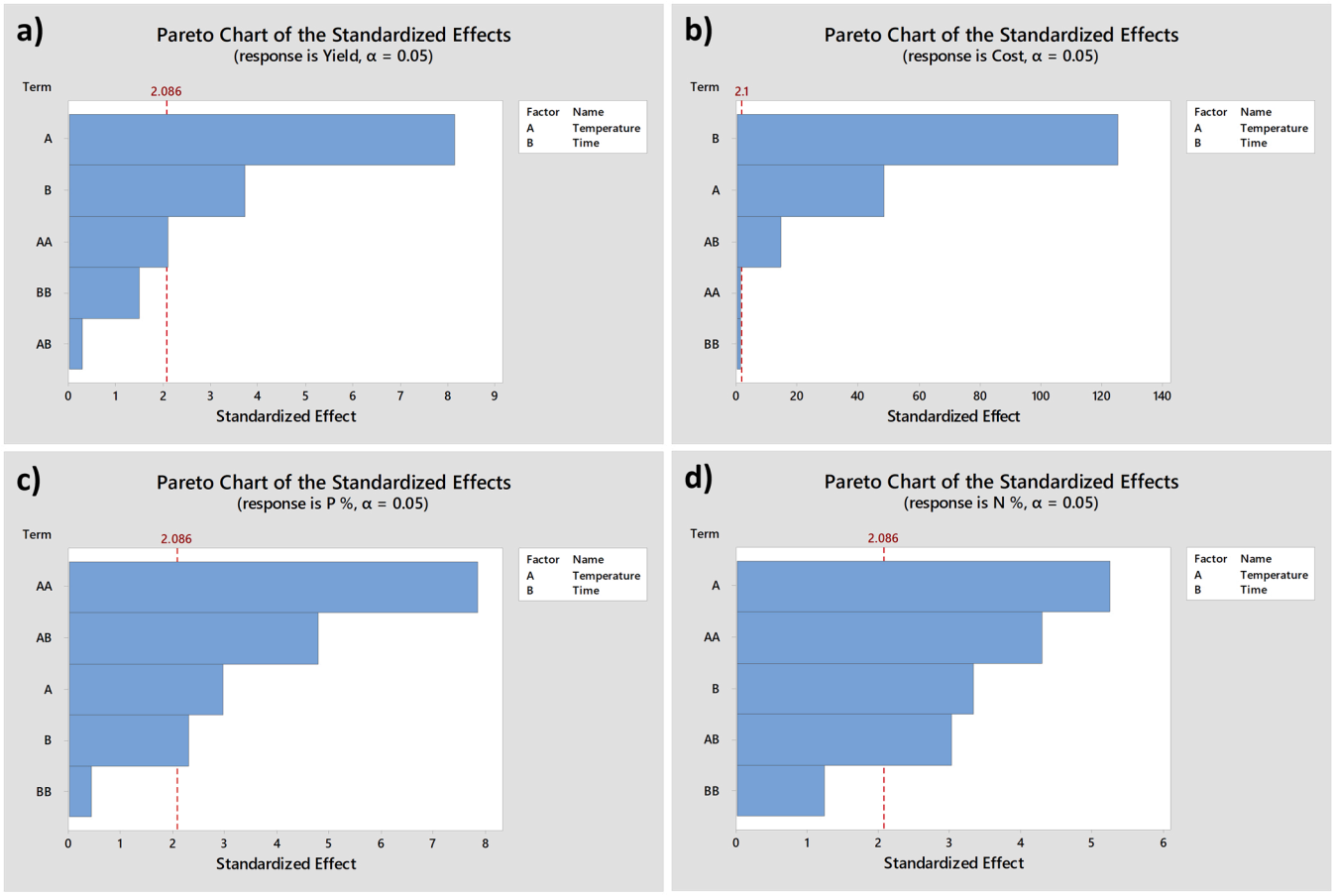

Fig. 2. Pareto chart of parameter effects using a central composite design (CCD) to consider pyrolysis yield (a), cost (b), PO_4^{3-}-P removal efficiency (c) and NH_4^+-N removal efficiency (d).

2.6. Experimental setup

One of the most frequently used second-order designs is central composite design (CCD) (Pagalan et al., 2020; Sahoo and Remya, 2020), which consists of three portions: a factorial (cube) portion (coded as −1, +1), an axial portion (coded as -α, + α), and n_0 centre points (Benredouane et al., 2016). Screening analysis by PBD showed the significant contribution of pyrolysis temperature (A) and time (B) on most of the responses (Y_x). The ranges of these two variables were therefore selected and a five-level CCD (Table 2) with 13 runs (26 when duplicated) (Table S2) was used to obtain the optimum level for the investigated variables.

The total number of experiments (N) were designed using Minitab software version 18.0 (Minitab Inc., USA) and graphically shown in SigmaPlot (Systat Software Inc. USA). The number of experiments were calculated as follows:

$$N = 2^k + 2k + n_0 = 4 + 4 + 5 = 13 \quad (4)$$

Where k is the factors number and n_0 is the number of central points. Therefore, the full factorial CCD for two variables contained 4 cube, 4 axial and five centre points, for a total of 13 experiments. The variables were coded as follows: temperature (500–800 °C) (A) and time (30–120 min) (B). The pyrolysis yield (Y_1), cost (Y_2), and removal efficiency for PO_4^{3-}-P (Y_3) and NH_4^+-N (Y_4) were selected as the process responses. The outcome of the statistical analysis was a fitted second-order polynomial in the form given below:

$$Y = \beta_0 + \sum_{i=1}^{k} \beta_i x_i + \sum_{i=1}^{k} \beta_{ii} (x_i)^2 + \sum_{i=1}^{k-1} \sum_{j=2}^{k} \beta_{ij} x_i x_j + \varepsilon \quad (5)$$

Where β_0 is a constant term, β_0, β_i; β_{ii}; β_{ij} are the regression coefficients (β_i is the linear coefficient, β_{ii} is the square coefficient, β_{ij} is the interactive coefficient); x_i and x_j are the coded values of variables, k is the variables number and ϵ is the residual error. The significance of the model was further analysed through an analysis of variance (ANOVA) (Show et al., 2020).

2.7. Preparation of the optimised biochar

The final optimised biochar is referred to here as OB (optimised biochar). This was prepared as follows. A mixed conifer brash (Lodgepole pine and Sitka spruce) was dried in the oven at 105 °C overnight. The dried brash was milled to ~0.1–1 mm with a mechanical mill (Retsch ZM 100) prior to pyrolysis. Known quantities of milled brash were placed into crucibles then into a muffle furnace (Carbolite CWF 1200) and heated from room temperature up to a final temperature of 500 °C, which was then held for 30 min. After cooling, the resultant biochar was rinsed with Milli-Q water to eliminate ash residues, then dried at 105 °C for 2 h and stored in plastic bags.

3. Results

3.1. Screening analysis

Five variables, namely, brash type (conifer species), pre-treatment, granulation, pyrolysis time and temperature were examined using the PBD to identify the key factors influencing the efficiency of the prepared biochars to adsorb PO_4^{3-}-P and NH_4^+-N from synthetic water solutions while maintaining the highest yield and the lowest cost. Fig. 1a-d shows

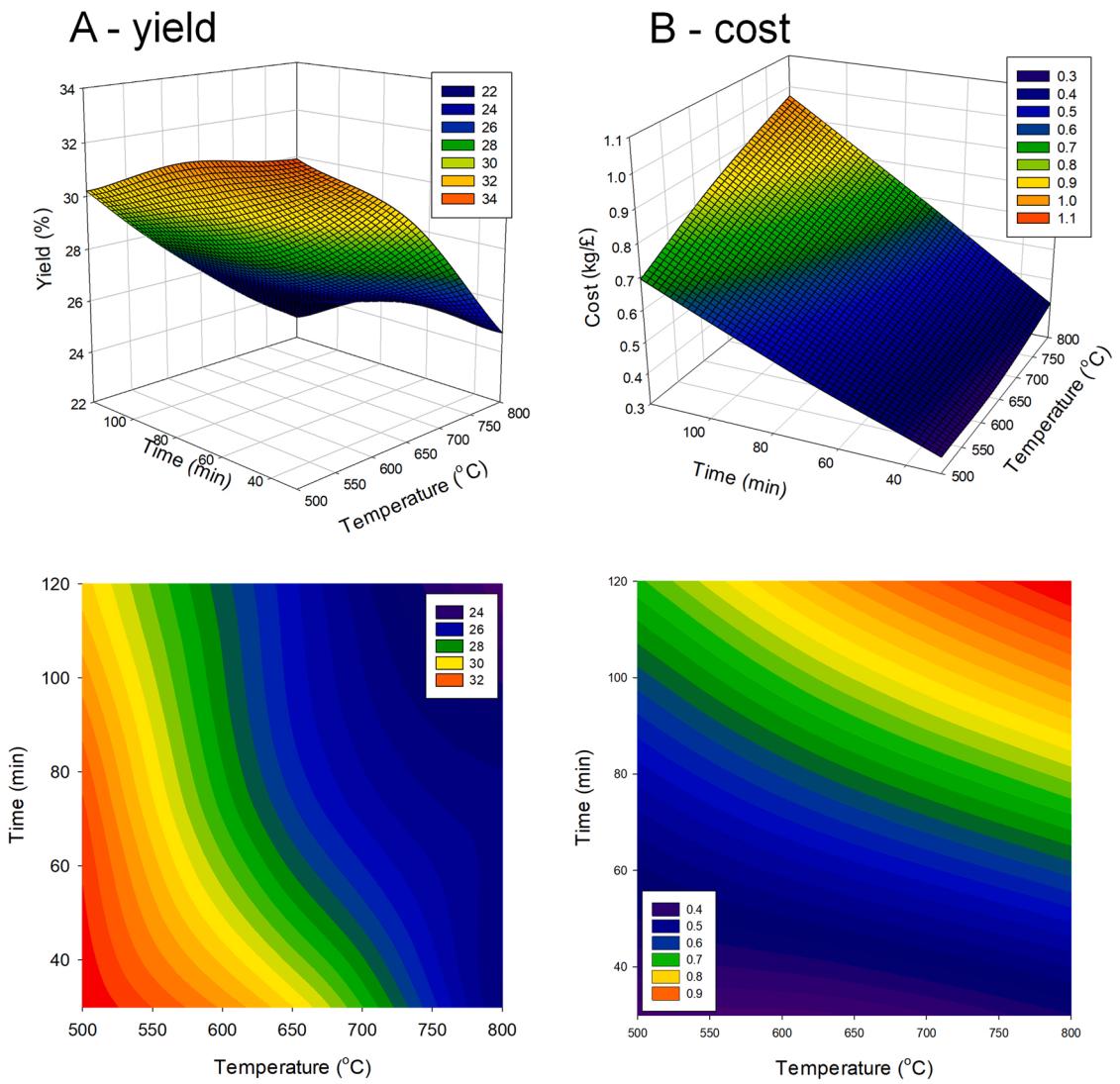

Fig. 3. Contour and three-dimensional response surface plots regarding the effects of time and temperature on yield (a), cost (b), PO_4^{3-}-P removal efficiency (c) and NH_4^+-N removal efficiency (d).

the Pareto charts for the standardised effects, which is a graphical illustration of the factorial elimination. For yield (a) and PO_4^{3-}-P removal (c), the pyrolysis temperature (E) had the highest influence (at the 0.05 ($P = 95$ %) significance level (Fig. 1)). Brash type (A) only slightly influenced PO_4^{3-}-P (c) removal but otherwise exerted no influence. The pyrolysis temperature (E) showed the most significant negative effect on yield (a) and positive effect on PO_4^{3-}-P removal (c). Pyrolysis time (D) and temperature (E) also had a significant negative effect on cost (b). NH_4^+-N removal (d) showed an unusual tendency since it was affected by granulation (C) and pretreatment (B). Based on these results and the complex relationship between the responses, pyrolysis temperature (E) and time (D) were selected for further optimisation (with CCD) as key variables, while the other three variables were kept constant (high significance) level. Tables S3–6 shows the ANOVA analysis, while Fig. S1 shows the residual plots from the screening analysis.

Eqs. (6–9) are the mathematical models established using multiple regression; these equations denote the empirical relationships between the responses (Y_{1-4}) and the variables (A-E) during the within the screening analysis using the Plackett–Burman design.

$$Y_1 = 85.73 + 1.72A + 3.01B - 9.59C - 0.1715D - 0.0844E \quad (6)$$

$$Y_2 = -0.21 - 0.0001A + 0.060B + 0.02C + 0.0046D + 0.0006E \quad (7)$$

$$Y_3 = -32.0 + 10.27A - 4.55B + 8.98C + 0.057D + 0.077E \quad (8)$$

$$Y_4 = 35.19 - 0.11A + 7.67B + 10.21C + 0.068D - 0.0014E \quad (9)$$

3.1.1. Central composite design (CCD)

The CCD matrix for the observed and predicted responses is shown in Table S2. Pareto charts (Fig. 2) revealed that both pyrolysis temperature (A) and time (B) singularly and in combination affected all responses (Y_x) except yield for AB. Temperature was a more consistent significant variable compared to time, i.e., generally $A > B$, except for cost. The BB model term was consistently classified as non-significant.

The expressions of the quadratic models developed for all responses are given in Eqs. (10–13).

$$Y_1 = 76.7 - 0.109A - 0.135B + 0.00006AA + 0.0005BB + 0.00004AB \quad (10)$$

$$Y_2 = 0.133 + 0.00022A + 0.00025B - 0.00AA - 0.00BB + 0.00AB \quad (11)$$

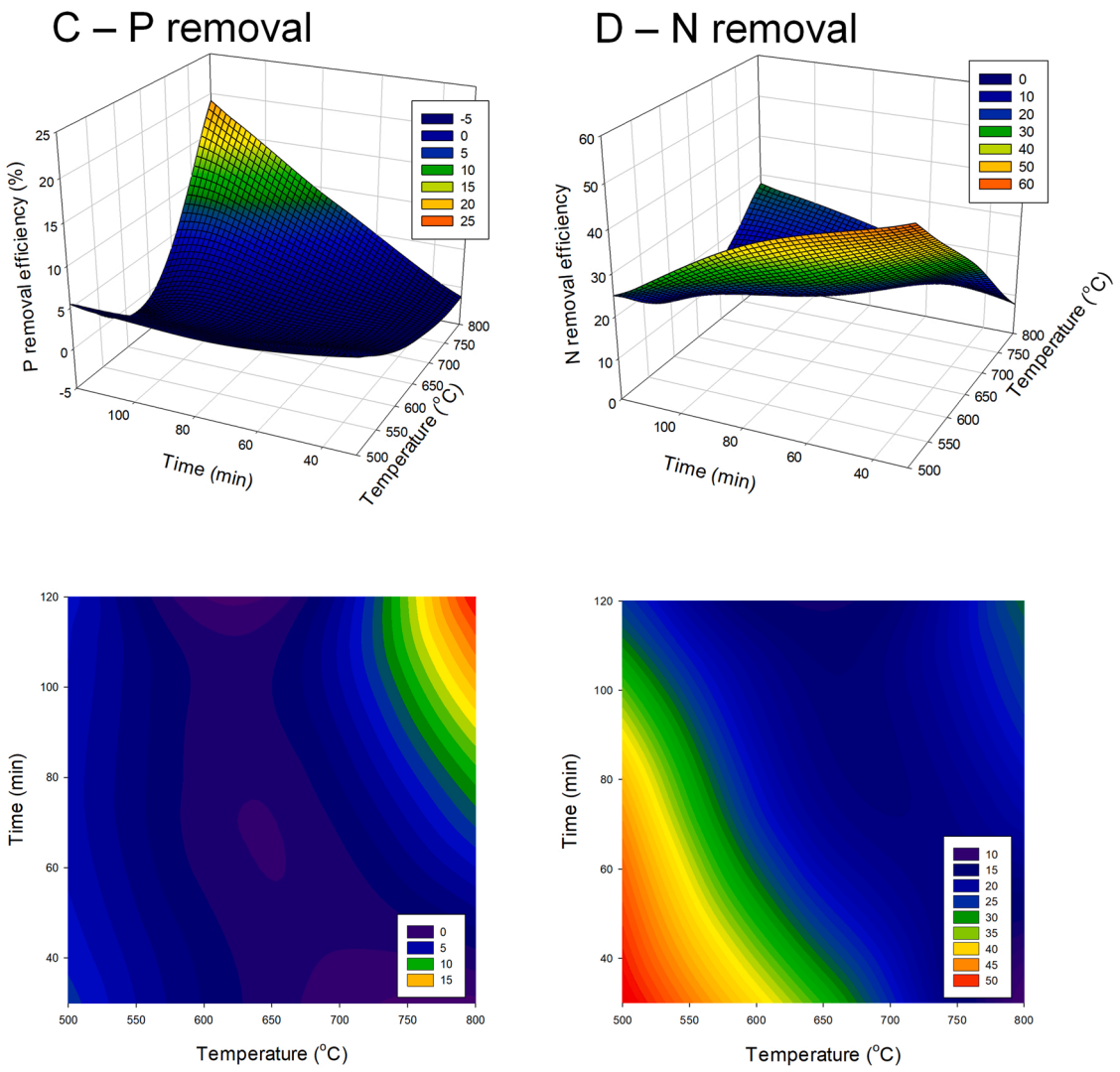

Fig. 3. (*continued*).

$$Y_3 = 162.4 - 0.452A - 0.538B + 0.0003AA + 0.0002BB + 0.0008AB \quad (12)$$

$$Y_4 = 431.3 - 0.993A - 1.650B + 0.0006AA + 0.0019BB + 0.0019AB \quad (13)$$

The variables A and B showed an antagonistic relationship with yield, PO_4^{3-}-P and NH_4^+-N removal efficiency. Further, ANOVA's for Y_1-Y_4 showed a p-value for models of 0.740, 0.000, 0.000 and 0.586, respectively, while high F-values indicated the quadratic models were highly significant (Table S7-10). The quadratic models correlation coefficients were relatively high $R^2 \geq 0.75$. The excellent correlation between the predicted and experimental results indicated a good relationship between the data (Table S2 and Fig. S2).

3.1.2. *Effects of interactive variables*

Three-dimensional response surfaces showing the relationship between responses (Y_x) and the variables (A-B) are shown in Fig. 3a-d. Yield (Fig. 3a) was mainly affected by pyrolysis temperature, while residence time had less effect. With increasing pyrolysis temperature, yield decreased. A similar tendency was observed for NH_4^+-N removal efficiency (Fig. 3d). Fig. 3b presents the influence of the two variables on biochar production cost. Cost increased when pyrolysis temperature and time increased. In the case of PO_4^{3-}-P removal efficiency the influence of the two variables was moderate, with no significant changes in removal efficiency over much of the studied interval (Fig. 3c); except at high temperatures (above 750 °C) and long pyrolosis (over 100 min) times – which showed a positive effect on PO_4^{3-}-P removal.

3.1.3. *Verification study*

The best possible experimental outcome (i.e., the highest PO_4^{3-}-P and NH_4^+-N removal efficiency and yield at the lowest cost) was determined using a desirability function method. To obtain the highest desirability (1.0) the pyrolysis temperature was assessed between 500 and 800 °C, while the pyrolysis time was between 30 and 120 min. The highest desirability was for A = 500 °C and B = 30 min, to achieve a maximum PO_4^{3-}-P removal of 9.93 %, with a desirability result of 0.86; NH_4^+-N removal of 65.21 %, with a result of 1.00; yield of 34.75 %, with a result of 1.00; and cost of 0.33 £ /kg, with a result of 1.00 (Fig. 4). The verification for the optimised biochar (OB) was investigated under optimal conditions, and the PO_4^{3-}-P and NH_4^+-N removal efficiencies obtained were 0 % and 63.58 %, respectively, while the yield was 34.78 % and the cost was 0.37 £ /kg (more details in Discussion). Table 3 shows the predicted and experimental values at these optimal conditions. From the results it can be concluded that the corresponding experimental values were near to the optimised predictions, except for PO_4^{3-}-P removal efficiency which failed to verify the developed model.

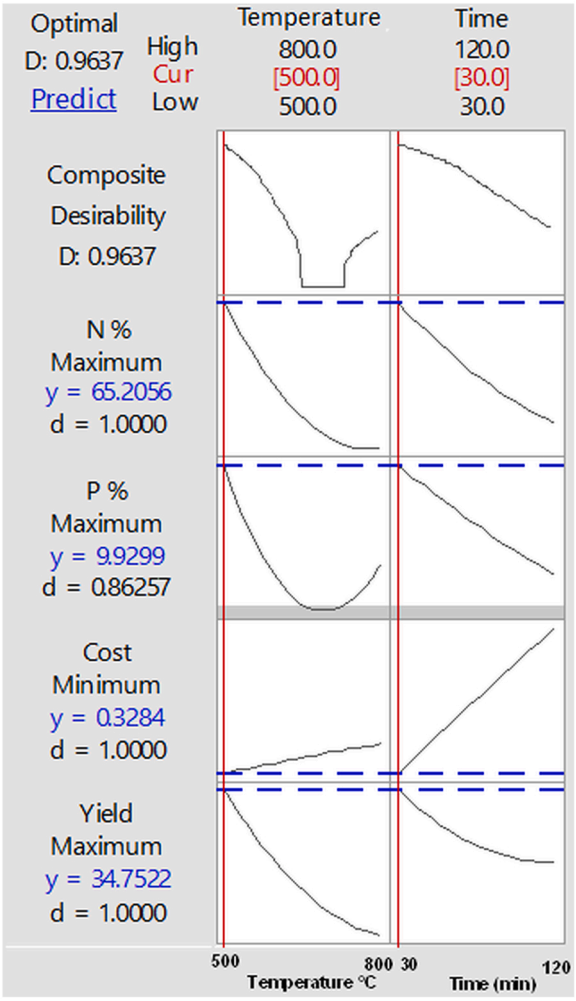

Fig. 4. Profiles for the predicated values and the desirability function for the Multiple Response Prediction. Red vertical lines show values after optimisation, i.e.; pyrolysis at 500 °C for 30 min to give the best possible outcome (highest PO_4^{3-}-P and NH_4^+-N removal efficiency, high yield and low cost), which are the target values (blue horizontal lines). (For interpretation of the references to colour in this figure legend, the reader is referred to the web version of this article.)

3.1.4. Characterisation

To better understand the PO_4^{3-}-P and NH_4^+-N removal behaviour with this OB, various characterisation methods and instrumental techniques were employed. The surface morphology of the OB was observed using SEM images, and elemental levels were estimated based on the EDX spectra alongside elemental mapping, as shown in Fig. 5a-d.

The SEM images in Fig. 5a-b show that the wood structure (from brash) was preserved after pyrolysis and the OB contained a porous structure with many regular and vertical channels. Results from the EDX pattern (Fig. 5c) demonstrated that C (81.8 %) and O (15.4 %) were the major elements in the OB structure, while other elements such K, Ca, P, Mg, Al, and Si were present in much lower percentages (<1 %). Further, EDX elemental mapping (Fig. 5d) confirmed that all the elements were uniformly present on the surface of the OB.

The biochar was of good quality, with a high volatile content and fixed carbon and low ash and moisture content (Table 4). The OB bulk density was low, at around 0.27 g/cm^3, but this can vary with feedstock and pyrolysis process conditions. Contact pH (pH_{sus}) relates to the overall content of acidic or basic functional groups of the OB (Paunovic et al., 2019). As the results in Table 4 show, the OB caused an increase in the pH of Milli-Q water (normally slightly acidic). This classifies it as a H-type biochar, hydrophobic in nature, which will adsorb mostly cationic compounds and increase the pH of neutral solutions (Sekulić et al., 2018).

The surface area and porosity of the OB was calculated using the Brunauer-Emmett-Teller (BET) equation as shown in Table 5. The BET surface area was 11.84 m^2/g. According to International Union of Pure and Applied Chemistry (IUPAC) classifications, the OB was meso/macroporous, with an average pore width of 3.71 nm (Table 5). Based on IUPAC isotherm classifications, the N_2 adsorption isotherm for the OB would be classified as Type II (Fig. 6a). The pore distribution curve for the OB decreased with increased pore width, and the pore diameter characteristics were all within 50 nm (Fig. 6a).

Fig. 6b shows the pH_{pzc} analysis of the OB by calculating the corresponding pH drift of KNO_3 solutions. The pH_{pzc} of the OB was calculated as 6.7. When the pH value in solution is less than 6.7, the surface of the OB is positively charged; when the pH value is greater than 6.7, the surface of the OB is negatively charged (Pap et al., 2018).

Fig. 6c presents the FTIR spectrums of the original biomass and the OB with the most notable functionalities observed. The FTIR spectra of the biomass exhibited the characteristic peaks for lignocellulosic wood biomass, while the OB showed the usual carbonous spectra for biochars. The band around 3300 cm^{-1} in the brash biomass spectra is related to —O—H and —N—H stretching vibration of the lignin. The peaks at 2900 cm^{-1} correspond to —C—H stretching compounds in the brash hemicellulose and cellulose. Peaks at 1730 cm^{-1} and 1600 cm^{-1} are assigned to the —C═O stretching in carboxylic groups (lactones and quinones) and carbon–carbon double bonds (—C═C) in the aromatic rings, respectively. The peaks around 1420 cm^{-1} correspond to CH_2 asymmetric bending, and aromatic —C—C stretching vibration. The bands between 1375 and 1100 cm^{-1} could be assigned to phenol —O—H peaks, —C—O vibration in carboxylic acids, amides, alcohols, and esters related to lignin. The band appearing at 1050 cm^{-1} is related to C—O—C bonds in cellulose and hemicellulose. Low-intensity bands between 900 and 600 cm^{-1} are assigned to aromatic C–H bending (Baysal et al., 2018; Šoštarić et al., 2018).

The OB spectra changed significantly due to dehydrogenation of carbohydrates, increases in aromatic structures and production of volatile organic matter (Fang et al., 2014; Kumar et al., 2021). The FTIR spectra of the OB shows an apparent loss of functionalisation in the region between 3500 and 1750 cm^{-1}, due to the loss of primary lignocellulosic structure and volatile aliphatic groups, while the aromatic compounds arises after dehydrogenation of carbohydrates and dominated the OB spectral features (Fig. 6a) (Liu et al., 2018).

The XRD pattern of the biomass and OB is given in Fig. 6d. The diffraction pattern of the biomass showed peaks located at 2θ between 15° and 22° which could be ascribed to the (0 0 2) plane of native cellulose I lattice. The weaker diffraction peak at 2θ of 15° was due to the existence of amorphous components (e.g., lignin and hemicellulose) (Rangabhashiyam et al., 2018; Tzvetkov et al., 2016). The intensity of this peak becomes lower after pyrolysis, whereas low and broad peaks for the OB are observed at around 23° and 44°, which attribute to

Table 3
Model validation parameters.

Temperature (°C)	Time (min)	Pyrolysis yield (%)		Production cost (£/kg)		Removal efficiency of PO_4^{3-}-P		Removal efficiency of NH_4^+-N	
		Predic.	Exper.	Predic.	Exper.	Predic.	Exper.	Predic.	Exper.
500	30	34.75	34.78	0.33	0.37	9.93	0.00	65.21	63.58

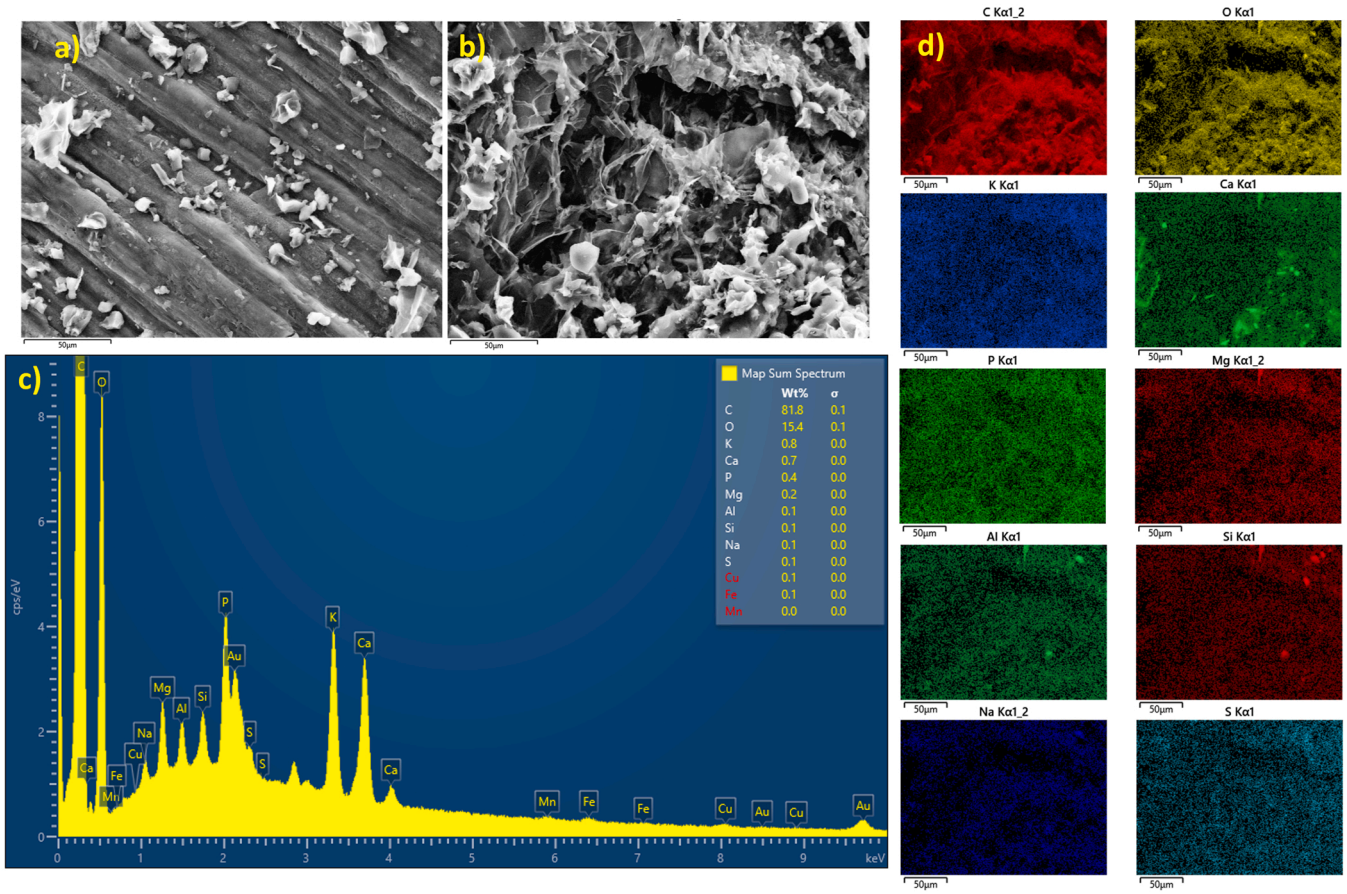

Fig. 5. SEM images (a) and (b) and SEM–EDX spectrum and elemental mapping images (c) and (d) of OB.

Table 4
Physico-chemical characterisation of the OB.

Biochar	Yield (%)	Moisture (%)	Volatiles (%)	Fixed carbon (%)	Ash (%)	pHsus	Bulk density (g/cm^3)
OB	34.78	2.4	24.6	71.9	1.1	8.85	0.27

Table 5
Brunauer-Emmett-Teller surface area analysis data for the OB.

Biochar	BET surface area (m^2/g)	External surface area (m^2/g)	Micropore volume (cm^3/g)	Average pore width (nm)
OB	11.84	0.87	0.006	3.71

diffraction of (0 0 2) and (1 0 0) planes of the graphite lattice in amorphous states. The diffraction of the (1 0 0) plane was scarcely visible which demonstrates the crystalline graphitisation to a certain degree (Taheran et al., 2016; Wang et al., 2015b). The OB contained mineral structures such as SiO_2 at 26.6° and $CaCO_3$ at 29.3° diffraction peaks.

To further probe the surface elemental composition of the OB, XPS analysis on the OB was carried out (Fig. 7a-d). Fig. 7a shows a survey scan for the OB with the surface element composition data. XPS analysis indicated a surface composition of C 83.6 at %, O 13.7 at % and N 2.7 at %. As shown in the XPS high resolution spectra of C1s (Fig. 7b), the three peaks at 284.78 (63 %) eV, 286.18 (17.5 %) eV and 289.08 (3.6%) eV were obtained for the OB and assigned to C—C, C—OH/C—OR and C═O, respectively (Zhao et al., 2019). The O1s spectra of the OB is shown in Fig. 7c, which involved two peaks at 531.48 (5.7 %) eV (assigned to O═C–O and carbonyl O═C groups), and 533.38 (6.9 %) eV (assigned to C—OH and O—C═O/CO_3^{2-}) (Herath et al., 2021). The N1s XPS spectrum in Fig. 7d indicates a small amount of nitrogen (compared to carbon and oxygen). The peak around 400 (3.3 %) eV is assigned to N1s, which relates to N—H and N—C (Yang and Jiang, 2014) forms of nitrogen.

Table 6
Estimated production cost of the optimised biochar (£/kg) here (Selvaraju and Bakar, 2017).

Components	Description	£ /kg
Cost of separation and transport (CST)	The raw material is locally and abundantly available. Difficult to predict, 10 % surcharge should be added to the overall cost.	0.02
Cost of drying raw material (CD)	Dried in oven, but could be air dried, which would reduce the cost.	0.12
Cost of size reduction (CSR)	The brash was crushed in a mechanical mill. The electricity consumption for 1 kg × cost of 1 unit = 0.1 × 0.08	0.08
Cost of the pyrolysis (CP)	Cost of pyrolysis = hours × temp units = 0.5 × 0.250	0.125
Cost of biochar washing (CW)	The biochar was washed with water.	0.02
Cost of drying the biochar (CDB)	Hours × units × per unit cost = 2 × 0.03 × 0.2	0.012

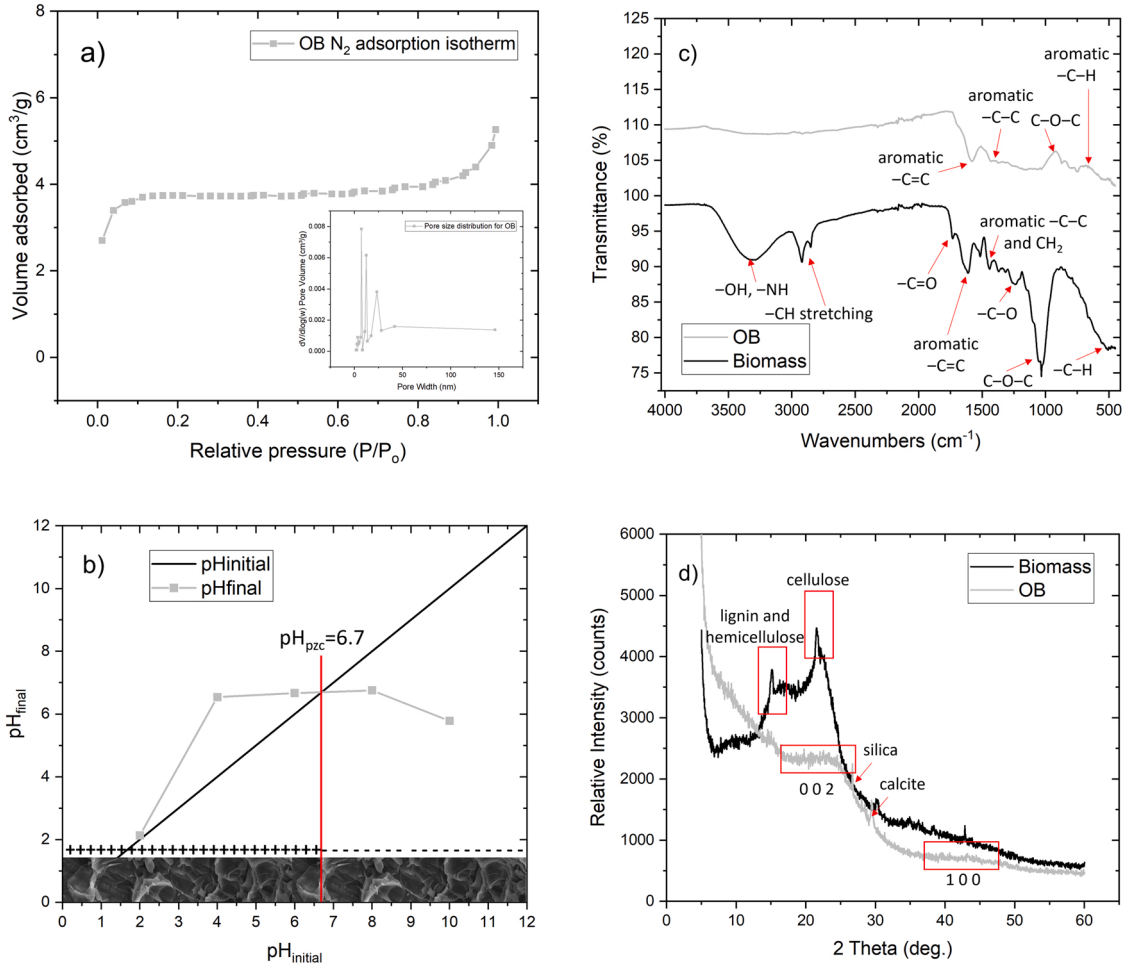

Fig. 6. BET isotherm with pore size distribution (a), pH_{pzc} curve (b), FTIR images (c) and XRD patterns (d) of raw biomass and OB.

4. Discussion

For optimal biochar yield, production techniques should not only consider biomass type and nature but also process conditions (e.g., temperature, residence time) (Cheng et al., 2021a). Conifer brash is a lignocellulosic biomass (wood waste) which maintains high production yields (Rangabhashiyam and Balasubramanian, 2019). Biochar yield generally decreases when temperature and residence time are increased during the pyrolysis process. Also, a reduction in biomass particle size (milling) results in lower biochar yield (Yaashikaa et al., 2020). The results from this study are in the line with these observations.

Biochar production cost is one of the most important aspects in the their marketing and application (Hu et al., 2021). To calculate the cost-effectiveness of biochar production, several factors are required including: feedstock cost (harvesting and storing), transport cost, pyrolysis cost, distribution cost, etc. (Oni et al., 2019). Despite an array of existing research, a major industrial biochar market is still absent, and practical biochar utilisation is progressing very slowly. This effectively limits the ability to make comprehensive biochar price comparisons (Vochozka et al., 2016). The unit cost (£/ton) for producing biochar from conifer brash here was predicted at 0.33 £ /kg (Table 3) and calculated at 0.37 £ /kg (Table 6). Pyrolysis temperature and time had the greatest impact on production costs through the use of electrical energy. The production cost of biochar (£/ton) in Scotland could be calculated following Eq. (4) – see Table 6 for components listed:

$$Biochar \quad cost \quad (£) = CST + CD + CSR + CP + CW + CDB \tag{14}$$

Maroušek and Trakal (2022) discussed various scenarios for biochar production from wood waste and estimated costs between 140 and 470 £ /ton, which is in line with the price determined here. Hence, one kg of conifer brash derived biochar may cost 0.37 £ /kg. This shows that the biochar is significantly cheaper than commercial activated carbon (up to 33.76 £/kg) and ion exchange resins (up to 110.8 £/kg) (Hu et al., 2020). Biomass (here brash) pyrolysis not only produces biochar, but also gaseous and liquid products. These by-products also have additional energetic and market value as fuels which could reduce biochar production costs further (Zhang et al., 2014, 2018).

Ammonium (NH_4^+) is one of the most common unoxidised inorganic forms of nitrogen in water (Hu et al., 2020). Based on the Emerson et al. (1975) calculation, NH_4^+ is the predominant (reduced) form (>90 %) in the aqueous phase at pH < 8.2 and temperatures < 28 °C, over ammonia (NH_3). To date, several biochars have been evaluated to remove NH_4^+-N, produced from different feedstocks and production conditions, e.g., fruit peal, maple wood, rice husk, corncob, cotton stalk and giant reed biochar. These have been produced at temperatures from 300° to 900°C and with residence times from 30 min to several hours (Yin et al., 2017). Generally, reported NH_4^+-N adsorption capacities are < 5 mg/g (and ~1 mg/g in this study). It has been observed that low-temperature biochars may have more negatively charged functionalities, and therefore a higher affinity toward positively charged NH_4^+-N. In this study, lower pyrolysis temperature increased NH_4^+-N removal efficiency and 500 °C was found as the optimised temperature for biochar production. A comparable result was achieved by Gai et al. (2014), who found that biochar pyrolysed at lower temperatures (400 °C and 500 °C) had higher NH_4^+-H removal efficiency than those pyrolysed at higher temperatures (600 °C and 700 °C). The surface chemistry of the OB here was largely

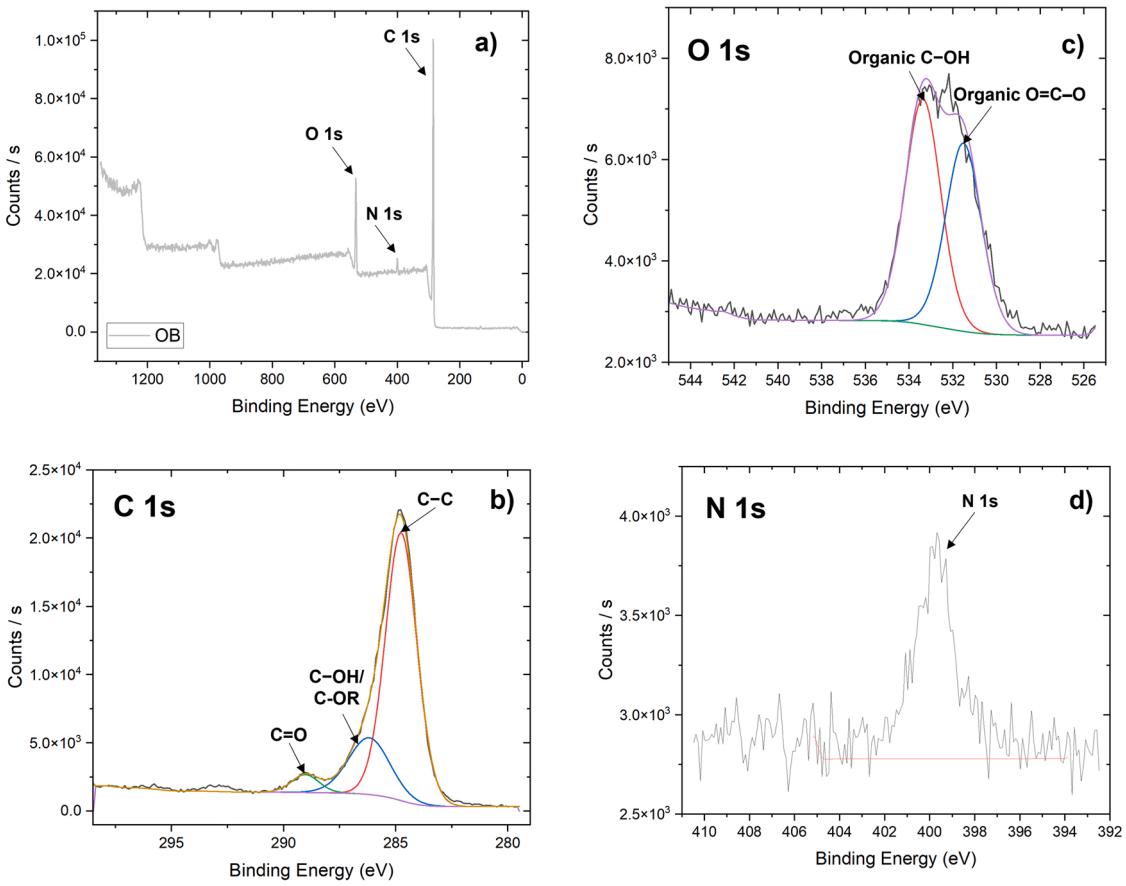

Fig. 7. XPS survey spectra (a) and high-resolution spectra of C 1 s (b), O 1 s (c) and N 1 s (d).

characterised by negatively charged surface functional groups (Fig. 6c and Fig. 7), most of them containing oxygen (e.g., —OH, —COOH). Consequently, the OB had affinity for NH_4^+-N through electrostatic attraction. Additionally, higher pyrolysis temperatures can increase biochar aromaticity and hydrophobicity (Zhang et al., 2020), thus reducing contact with hydrophilic NH_4^+-N (Yin et al., 2019). The outer-sphere complexation of NH_4^+-N onto the OB surfaces here, would result in interactions with O-containing functional groups to form amines and amides, as NH_4^+-N acts as a Brønsted or Lewis acid (Wang et al., 2015a). Furthermore, pH is one of the most important parameters in adsorption. The OB here had a high pH (8.85), which additionally resulted in NH_4^+-N solution pH increasing after adsorption (data not shown). At this pH (pH < 9) functional groups on the OB surface had negative charges which bonded the NH_4^+-N.

Inorganic P in aqueous solutions is present in several anionic forms, such as $H_2PO_4^-$, HPO_4^{2-}, and PO_4^{3-}, depending on pH and Eh. The majority of studies demonstrate that raw/unmodified biochars have no, or very low, adsorption capacity for PO_4^{3-}-P (Zhang et al., 2020), since PO_4^{3-}-P anions are largely repelled by the negatively charged biochar surfaces. A slight increase in removal efficiency of PO_4^{3-}-P at higher pyrolysis temperatures here could be attributed to an increase in biochar surface area and changes in surface chemistry (i.e., loss of O-containing polar functional groups causing alkaline characteristics). A more alkaline biochar could be produced at higher temperatures due to the fact that the ash content in the biochar increases. Meanwhile, the acidic substances in biochar would be volatilised (Lou et al., 2016). The net charge on the OB surface here was negative at the conditions used (7 < solution pH < 9) which resulted in the CCD model verification failing. Since the optimisation procedure was designed to achieve the best results for all four responses simultaneously, although higher pyrolysis temperatures were desirable for P, it was determined that 500 °C gave maximum yield, low cost and maximum NH_4^+-N removal. Cui et al. (2016) evaluated the adsorption capacity of PO_4^{3-}-P for more than twenty biochars derived from wetland biomass. Only four biochars showed affinity toward PO_4^{3-}-P, indicating almost no pre-existing interactions. In addition, some desorption/leaching of PO_4^{3-}-P from biochars was observed in some studies due to endogenous P, which was a characteristic for our study as well (Table S2). In this case, biochar may become a nutrient (P) source. Recent research has shown that inherent or added alkali metals (metal oxides and hydroxides) can dramatically alter the leaching of nutrients from biochar and increase the adsorption capacity of P and N, which has important implications for the engineering of biochar for water treatment applications (Zhang et al., 2020).

4.1. Potential for brash-biochar production from forest-to-bog restoration sites

Originally, it was proposed that biochar produced from waste brash could potentially be a marketable water treatment product, or, used in forest-to-bog restoration sites in watercourses (e.g., drains) to remove excess nutrients which are released following restoration (i.e., from physical disturbance, peat rewetting and brash and needle decomposition; Gaffney et al., 2022). Our results suggest that biochar produced from waste brash does not remove sufficient quantities of NH_4^+-N and PO_4^{3-}-P from solution, in an unmodified form. Thus, at present, it is not beneficial as a targeted water treatment product in restoration sites for this purpose. However, peatland restoration is a growing global practice that aims to improve ecosystem services such as climate regulation, water provision and biodiversity conservation. Restoration of afforested peatland has multiple positive outcomes, such as reduction in soil CO_2 emissions (due to increased water table and reduced aeration); uptake of CO_2 (due to increase in C stock in ground vegetation); resumption of net

C sequestration in peat (if peat formation/accumulation reinstates) – all of which occur over the longer term (Gaffney et al., 2022). As an additional by-product of peatland deforestation and restoration, waste brash can be converted to biochar. This then has the potential to be used in other settings, even if it has limited efficacy in raw form for nutrient run-off abatement. By converting readily degradable wood waste to biochar – not only is a potential source of nutrient run-off removed from a system, but a stable form of solid carbon is generated which in itself could act as an extra carbon pool within a restored peatland or other soil environment.

Further, by modifying the surface chemistry of a biochar (e.g., by incorporation of alkali metals such as Mg, Mn, Ce, La and Zr) the adsorption capacity (and thus removal efficiency) for NH_4^+-N and PO_4^{3-}-P could be increased, allowing significant quantities of each to be removed from solution (Shakoor et al., 2021; Vikrant et al., 2018). In general, modification increases biochar production costs, the extent to which depends on the metals used and the additional energy costs needed. The addition of alkali metals to biochar may also bring with it increased environmental risk, in terms of metal leaching and toxicity (Zhi et al., 2020). Therefore, financial costs, environmental risks and any net benefits to restoration sites should be considered in future research work.

5. Conclusion

In attempting to create a more 'circular economy' approach to waste conifer brash management following removal of trees from afforested peatland sites, this study investigated the potential removal of nitrogen (NH_4^+-N) and phosphorus (PO_4^{3-}-P) from water via adsorption using unmodified biochar made from conifer brash (OB). The results show that this OB weakly adsorbed NH_4^+-N, while PO_4^{3-}P was not removed. For anionic PO_4^{3-}P, this was due to electrostatic repulsion elicited by the negatively charged biochar surface. Removal efficiencies were explained through extensive OB characterisation. To enhance the adsorption capability of this OB for N and P removal, surface modification (functionalisation) of the biochar would be necessary to reduce electrostatic repulsion or enhance surface interactions. The cost and environmental risk of biochar modification need to be explored in future research. Without further modification, this OB was not beneficial for use in targeted water treatment (N or P removal) at restoration sites, however, its creation from wood waste at peatland restoration sites would remove a significant biodegradable waste biomass and nutrient source. Additionally, creation of such a biochar may form a value-added product that could help to offset the costs of 'forest to bog' peatland restoration in certain scenarios.

CRediT authorship contribution statement

Sabolc Pap: Conceptualisation, Investigation, Methodology, Validation, Formal analysis, Visualisation, Writing – original draft, Writing – review & editing, Funding acquisition, Project administration. **Paul P.J. Gaffney:** Conceptualisation, Investigation, Methodology, Validation, Formal analysis, Visualisation, Writing – original draft, Writing – review & editing, Funding acquisition, Project administration. **Qunying Zhao:** Formal analysis, Investigation. **Daniela Klein**: Writing – review & editing. **Yuan Li:** Formal analysis. **Caroline Kirk:** Formal analysis, Investigation, Writing – review & editing. **Mark A. Taggarta:** Supervision, Writing – review & editing.

Declaration of Competing Interest

The authors declare that they have no known competing financial interests or personal relationships that could have appeared to influence the work reported in this paper.

Acknowledgements

We gratefully acknowledge financial support from: the RSPB Forsinard Flows National Nature Reserve; the University of the Highlands and Islands WaterHub Challenge Fund; the Natural Science Foundation of Education Department of Shaanxi Province (Grant No: 18JK0375); The Royal Society of Chemistry 'RSC Research Fund' (Grant R20-7810); and the Royal Society Research Grants Scheme 2021 (Grant RGS\R1 \211266). We thank Darrell Stevens, Neil Cowie (RSPB) and Roxane Andersen (UHI) for supporting conception and development of this project.

Appendix A. Supporting information

Supplementary data associated with this article can be found in the online version at doi:10.1016/j.indcrop.2022.115165.

References

Anderson, R., Vasander, H., Geddes, N., Laine, A., Tolvanen, A., O'sullivan, A., Aapala, K., 2016. Afforested and forestry-drained peatland restoration, in: Bonn, A. (Ed.), Peatland Restoration and Ecosystem Services: Science, Policy and Practice. Cambridge Univeristy Press, Cambridge, pp. 213–233. https://doi.org/10.1017/CBO9781139177788.013.

APHA, 2005. Standard methods for the examination of water and wastewater, APHA, AWWA, and WPCE. Am. Public Heal. Assoc. Springfield, New York Byrd Prog.

Baysal, M., Bilge, K., Yılmaz, B., Papila, M., Yürüm, Y., 2018. Preparation of high surface area activated carbon from waste-biomass of sunflower piths: kinetics and equilibrium studies on the dye removal. J. Environ. Chem. Eng. 6, 1702–1713. https://doi.org/10.1016/j.jece.2018.02.020.

Benredouane, S., Berrama, T., Doufene, N., 2016. Strategy of screening and optimization of process parameters using experimental design: application to amoxicillin elimination by adsorption on activated carbon. Chemom. Intell. Lab. Syst. 155, 128–137. https://doi.org/10.1016/j.chemolab.2016.04.010.

Bonn, A., Allott, T., Evans, M., Joosten, H., Stoneman, R., 2016. Peatland Restoration and Ecosystem Services: Science, Policy and Practice. Cambridge University Press.

Bubier, J.L., Moore, T.R., Bledzki, L.A., 2007. Effects of nutrient addition on vegetation and carbon cycling in an ombrotrophic bog. Glob. Chang. Biol. 13, 1168–1186. https://doi.org/10.1111/j.1365-2486.2007.01346.x.

Bursztyn Fuentes, A.L., Canevesi, R.L.S., Gadonneix, P., Mathieu, S., Celzard, A., Fierro, V., 2020. Paracetamol removal by Kon-Tiki kiln-derived biochar and activated carbons. Ind. Crops Prod. 155, 112740 https://doi.org/10.1016/j.indcrop.2020.112740.

Cheng, Jiali, Li, X., Xiao, X., Yuan, Y., Liao, X., Shi, B., Zhang, S., Ao, Z., 2021. Metal oxide loaded biochars derived from Chinese bai jiu distillers' grains used for the adsorption and controlled release of phosphate. Ind. Crops Prod. 173, 114080 https://doi.org/10.1016/j.indcrop.2021.114080.

Cheng, Jie, Hu, S.C., Sun, G.T., Geng, Z.C., Zhu, M.Q., 2021. The effect of pyrolysis temperature on the characteristics of biochar, pyroligneous acids, and gas prepared from cotton stalk through a polygeneration process. Ind. Crops Prod. 170, 113690 https://doi.org/10.1016/j.indcrop.2021.113690.

Cui, X., Hao, H., He, Z., Stoffella, P.J., Yang, X., 2016. Pyrolysis of wetland biomass waste: potential for carbon sequestration and water remediation. J. Environ. Manag. 173, 95–104. https://doi.org/10.1016/j.jenvman.2016.02.049.

Emerson, K., Russo, R.C., Lund, R.E., Thurston, R.V., 1975. Aqueous ammonia equilibrium calculations: effect of pH and temperature. J. Fish. Board Can. 32, 2379–2383.

Fang, Q., Chen, B., Lin, Y., Guan, Y., 2014. Aromatic and hydrophobic surfaces of wood-derived biochar enhance perchlorate adsorption via hydrogen bonding to oxygen-containing organic groups. Environ. Sci. Technol. 48, 279–288. https://doi.org/10.1021/es403711y.

Fatima, I., Ahmad, M., Vithanage, M., Iqbal, S., 2021. Abstraction of nitrates and phosphates from water by sawdust- and rice husk-derived biochars: their potential as N- and P-loaded fertilizer for plant productivity in nutrient deficient soil. J. Anal. Appl. Pyrolysis 155, 105073. https://doi.org/10.1016/j.jaap.2021.105073.

Gaffney, P.P.J., Hancock, M.H., Taggart, M.A., Andersen, R., 2018. Measuring restoration progress using pore- and surface-water chemistry across a chronosequence of formerly afforested blanket bogs. J. Environ. Manag. 219, 239–251.

Gaffney, P.P.J., Hancock, M.H., Taggart, M.A., Andersen, R., 2021. Catchment water quality in the year preceding and immediately following restoration of a drained afforested blanket bog. Biogeochemistry 153, 243–262.

Gaffney, P.P.J., Hancock, M.H., Taggart, M.A., Andersen, R., 2022. Restoration of afforested peatland: effects on pore- and surface-water quality in relation to differing harvesting methods. Ecol. Eng. 177, 106567.

Gai, X., Wang, H., Liu, J., Zhai, L., Liu, S., Ren, T., Liu, H., 2014. Effects of feedstock and pyrolysis temperature on biochar adsorption of ammonium and nitrate. PLoS One 9, e113888.

Gao, Y., Wang, B., Luo, L., Deng, B., Shad, N., Hu, D., Aly, H.M., Zhang, L., 2022. Effects of hydroxyapatite and modified biochar derived from Camellia oleifera fruit shell on

soil Cd contamination and N2O emissions. Ind. Crops Prod. 177, 114476 https://doi.org/10.1016/j.indcrop.2021.114476.
Guo, J., Yang, S., He, Q., Chen, Y., Zheng, F., Zhou, H., Hou, C., Du, B., Jiang, S., Li, H., 2021. Improving benzo(a)pyrene biodegradation in soil with wheat straw-derived biochar amendment: performance, microbial quantity, CO_2 emission, and soil properties. J. Anal. Appl. Pyrolysis 156, 105132. https://doi.org/10.1016/j.jaap.2021.105132.
Hambley, G., Andersen, R., Levy, P., Saunders, M., Cowie, N.R., Teh, Y.A., Hill, T.C., 2019. Net ecosystem exchange from two formerly afforested peatlands undergoing restoration in the Flow Country of northern Scotland. Mires Peat 23, 1–14. https://doi.org/10.19189/MaP.2018.DW.346.
Hancock, M.H., Klein, D., Andersen, R., Cowie, N.R., 2018. Vegetation response to restoration management of a blanket bog damaged by drainage and afforestation. Appl. Veg. Sci. 1–11.
Herath, A., Layne, C.A., Perez, F., Hassan, E.B., Pittman, C.U., Mlsna, T.E., 2021. KOH-activated high surface area Douglas Fir biochar for adsorbing aqueous Cr(VI), Pb(II) and Cd(II). Chemosphere 269, 128409. https://doi.org/10.1016/j.chemosphere.2020.128409.
Hu, Q., Jung, J., Chen, D., Leong, K., Song, S., Li, F., Mohan, B.C., Yao, Z., Prabhakar, A. K., Lin, X.H., Lim, E.Y., Zhang, L., Souradeep, G., Ok, Y.S., Kua, H.W., Li, S.F.Y., Tan, H.T.W., Dai, Y., Tong, Y.W., Peng, Y., Joseph, S., Wang, C.H., 2021. Biochar industry to circular economy. Sci. Total Environ. 757, 143820 https://doi.org/10.1016/j.scitotenv.2020.143820.
Hu, X., Zhang, X., Ngo, H.H., Guo, W., Wen, H., Li, C., Zhang, Y., Ma, C., 2020. Comparison study on the ammonium adsorption of the biochars derived from different kinds of fruit peel. Sci. Total Environ. 707, 135544 https://doi.org/10.1016/j.scitotenv.2019.135544.
Kumar, N.S., Shaikh, H.M., Asif, M., Al-Ghurabi, E.H., 2021. Engineered biochar from wood apple shell waste for high-efficient removal of toxic phenolic compounds in wastewater. Sci. Rep. 11, 1–17. https://doi.org/10.1038/s41598-021-82277-2.
Liu, Y., Ma, S., Chen, J., 2018. A novel pyro-hydrochar via sequential carbonization of biomass waste: preparation, characterization and adsorption capacity. J. Clean. Prod. 176, 187–195. https://doi.org/10.1016/j.jclepro.2017.12.090.
Lou, K., Rajapaksha, A.U., Ok, Y.S., Chang, S.X., 2016. Pyrolysis temperature and steam activation effects on sorption of phosphate on pine sawdust biochars in aqueous solutions. Chem. Speciat. Bioavailab. 28, 42–50. https://doi.org/10.1080/09542299.2016.1165080.
Maroušek, J., Trakal, L., 2022. Techno-economic analysis reveals the untapped potential of wood biochar. Chemosphere 291. https://doi.org/10.1016/j.chemosphere.2021.133000.
Mood, S.H., Ayiania, M., Cao, H., Marin-flores, O., Milan, Y.J., Garcia-perez, M., 2021. Nitrogen and magnesium Co-doped biochar for phosphate adsorption. Biomass Convers. Biorefin.
Oginni, O., Singh, K., 2021. Effect of carbonization temperature on fuel and caffeine adsorption characteristics of white pine and Norway spruce needle derived biochars. Ind. Crops Prod. 162, 113261 https://doi.org/10.1016/j.indcrop.2021.113261.
Oni, B.A., Oziegbe, O., Olawole, O.O., 2019. Significance of biochar application to the environment and economy. Ann. Agric. Sci. 64, 222–236. https://doi.org/10.1016/j.aoas.2019.12.006.
Pagalan, E., Sebron, M., Gomez, S., Salva, S.J., Ampusta, R., Macarayo, A.J., Joyno, C., Ido, A., Arazo, R., 2020. Activated carbon from spent coffee grounds as an adsorbent for treatment of water contaminated by aniline yellow dye. Ind. Crops Prod. 145, 111953 https://doi.org/10.1016/j.indcrop.2019.111953.
Pap, S., Bezanovic, V., Radonic, J., Babic, A., Saric, S., Adamovic, D., Turk Sekulic, M., 2018. Synthesis of highly-efficient functionalized biochars from fruit industry waste biomass for the removal of chromium and lead. J. Mol. Liq. 268, 315–325. https://doi.org/10.1016/j.molliq.2018.07.072.
Pap, S., Boyd, K.G., Taggart, M.A., Sekulic, M.T., 2021a. Circular economy based landfill leachate treatment with sulphur-doped microporous biochar. Waste Manag. https://doi.org/10.1016/j.wasman.2021.01.037.
Pap, S., Stankovits, G.J., Gyalai-Korpos, M., Makó, M., Erdélyi, I., Turk Sekulic, M., 2021b. Biochar application in organics and ultra-violet quenching substances removal from sludge dewatering leachate for algae production. J. Environ. Manag. 298. https://doi.org/10.1016/j.jenvman.2021.113446.
Paunovic, O., Pap, S., Maletic, S., Taggart, M.A., Boskovic, N., Turk Sekulic, M., 2019. Ionisable emerging pharmaceutical adsorption onto microwave functionalised biochar derived from novel lignocellulosic waste biomass. J. Colloid Interface Sci. 547, 350–360. https://doi.org/10.1016/j.jcis.2019.04.011.
Rana, A.K., Mishra, Y.K., Gupta, V.K., Thakur, V.K., 2021. Sustainable materials in the removal of pesticides from contaminated water: perspective on macro to nanoscale cellulose. Sci. Total Environ. 797, 149129 https://doi.org/10.1016/j.scitotenv.2021.149129.
Rana, A.K., Gupta, V.K., Newbold, J., Roberts, D., Rees, R.M., Krishnamurthy, S., Thakur, V.K., 2022. Sugar beet pulp: resurgence and trailblazing journey towards a circular bioeconomy. Fuel 312, 122953. https://doi.org/10.1016/j.fuel.2021.122953.
Rangabhashiyam, S., Balasubramanian, P., 2019. The potential of lignocellulosic biomass precursors for biochar production: performance, mechanism and wastewater application—A review. Ind. Crops Prod. 128, 405–423. https://doi.org/10.1016/j.indcrop.2018.11.041.
Rangabhashiyam, S., Lata, S., Balasubramanian, P., 2018. Biosorption characteristics of methylene blue and malachite green from simulated wastewater onto Carica papaya wood biosorbent. Surf. Interfaces 10, 197–215. https://doi.org/10.1016/j.surfin.2017.09.011.
Sahoo, D., Remya, N., 2020. Influence of operating parameters on the microwave pyrolysis of rice husk: biochar yield, energy yield, and property of biochar. Biomass Convers. Biorefin. https://doi.org/10.1007/s13399-020-00914-8.
Selvaraju, G., Bakar, N.K.A., 2017. Production of a new industrially viable green-activated carbon from Artocarpus integer fruit processing waste and evaluation of its chemical, morphological and adsorption properties. J. Clean. Prod. 141, 989–999. https://doi.org/10.1016/j.jclepro.2016.09.056.
Shah, N., Nisbet, T., 2019. The effects of forest clearance for peatland restoration on water quality. Sci. Total Environ. 693, 133617.
Shakoor, M.B., Ye, Z.L., Chen, S., 2021. Engineered biochars for recovering phosphate and ammonium from wastewater: a review. Sci. Total Environ. 779, 146240 https://doi.org/10.1016/j.scitotenv.2021.146240.
Show, S., Karmakar, B., Halder, G., 2020. Sorptive uptake of anti-inflammatory drug ibuprofen by waste biomass–derived biochar: experimental and statistical analysis. Biomass Convers. Biorefin. https://doi.org/10.1007/s13399-020-00922-8.
Šoštarić, T.D., Petrović, M.S., Pastor, F.T., Lončarević, D.R., Petrović, J.T., Milojković, J. V., Stojanović, M.D., 2018. Study of heavy metals biosorption on native and alkali-treated apricot shells and its application in wastewater treatment. J. Mol. Liq. 259, 340–349. https://doi.org/10.1016/j.molliq.2018.03.055.
Suryawanshi, S.S., Kamble, P.P., Gurav, R., Yang, Y.H., Jadhav, J.P., 2021. Statistical comparison of various agricultural and non-agricultural waste biomass-derived biochar for methylene blue dye sorption. Biomass Convers. Biorefin. https://doi.org/10.1007/s13399-021-01636-1.
Taheran, M., Naghdi, M., Brar, S.K., Knystautas, E.J., Verma, M., Ramirez, A.A., Surampalli, R.Y., Valero, J.R., 2016. Adsorption study of environmentally relevant concentrations of chlortetracycline on pinewood biochar. Sci. Total Environ. 571, 772–777. https://doi.org/10.1016/j.scitotenv.2016.07.050.
Turk Sekulić, M., Pap, S., Stojanović, Z., Bošković, N., Radonić, J., Šolević Knudsen, T., 2018. Efficient removal of priority, hazardous priority and emerging pollutants with Prunus armeniaca functionalized biochar from aqueous wastes: experimental optimization and modeling. Sci. Total Environ. 613–614, 736–750. https://doi.org/10.1016/j.scitotenv.2017.09.082.
Tzvetkov, G., Mihaylova, S., Stoitchkova, K., Tzvetkov, P., Spassov, T., 2016. Mechanochemical and chemical activation of lignocellulosic material to prepare powdered activated carbons for adsorption applications. Powder Technol. 299, 41–50. https://doi.org/10.1016/j.powtec.2016.05.033.
Vikrant, K., Kim, K.H., Ok, Y.S., Tsang, D.C.W., Tsang, Y.F., Giri, B.S., Singh, R.S., 2018. Engineered/designer biochar for the removal of phosphate in water and wastewater. Sci. Total Environ. 616–617, 1242–1260. https://doi.org/10.1016/j.scitotenv.2017.10.193.
Vochozka, M., Maroušková, A., Váchal, J., Straková, J., 2016. Biochar pricing hampers biochar farming. Clean. Technol. Environ. Policy 18, 1225–1231. https://doi.org/10.1007/s10098-016-1113-3.
Vu, N.T., Do, K.U., 2021. Insights into adsorption of ammonium by biochar derived from low temperature pyrolysis of coffee husk. Biomass Convers. Biorefin. https://doi.org/10.1007/s13399-021-01337-9.
Wang, B., Lehmann, J., Hanley, K., Hestrin, R., Enders, A., 2015. Adsorption and desorption of ammonium by maple wood biochar as a function of oxidation and pH. Chemosphere 138, 120–126. https://doi.org/10.1016/j.chemosphere.2015.05.062.
Wang, K., Zhao, N., Lei, S., Yan, R., Tian, X., Wang, J., Song, Y., Xu, D., Guo, Q., Liu, L., 2015. Promising biomass-based activated carbons derived from willow catkins for high performance supercapacitors. Electrochim. Acta 166, 1–11. https://doi.org/10.1016/j.electacta.2015.03.048.
Wilson, J.D., Anderson, R., Bailey, S., Chetcuti, J., Cowie, N.R., Hancock, M.H., Quine, C. P., Russell, N., Stephen, L., Thompson, D.B.A., 2014. Modelling edge effects of mature forest plantations on peatland waders informs landscape-scale conservation. J. Appl. Ecol. 51, 204–213. https://doi.org/10.1111/1365-2664.12173.
Yaashikaa, P.R., Kumar, P.S., Varjani, S., Saravanan, A., 2020. A critical review on the biochar production techniques, characterization, stability and applications for circular bioeconomy. Biotechnol. Rep. 28, e00570 https://doi.org/10.1016/j.btre.2020.e00570.
Yang, G.X., Jiang, H., 2014. Amino modification of biochar for enhanced adsorption of copper ions from synthetic wastewater. Water Res 48, 396–405. https://doi.org/10.1016/j.watres.2013.09.050.
Yin, Q., Zhang, B., Wang, R., Zhao, Z., 2017. Biochar as an adsorbent for inorganic nitrogen and phosphorus removal from water: a review. Environ. Sci. Pollut. Res. 24, 26297–26309. https://doi.org/10.1007/s11356-017-0338-y.
Yin, Q., Liu, M., Ren, H., 2019. Biochar produced from the co-pyrolysis of sewage sludge and walnut shell for ammonium and phosphate adsorption from water. J. Environ. Manag. 249, 109410 https://doi.org/10.1016/j.jenvman.2019.109410.
Zhang, M., Song, G., Gelardi, D.L., Huang, L., Khan, E., Mašek, O., Parikh, S.J., Ok, Y.S., 2020. Evaluating biochar and its modifications for the removal of ammonium, nitrate, and phosphate in water. Water Res. 186. https://doi.org/10.1016/j.watres.2020.116303.
Zhang, X., Zhang, S., Yang, H., Feng, Y., Chen, Y., Wang, X., Chen, H., 2014. Nitrogen enriched biochar modified by high temperature CO_2-ammonia treatment: characterization and adsorption of. Chem. Eng. J. 257 (20–27), CO2. https://doi.org/10.1016/j.cej.2014.07.024.
Zhang, Xiong, Che, Q., Cui, X., Wei, Z., Zhang, Xiaoyan, Chen, Y., Wang, X., Chen, H., 2018. Application of biomass pyrolytic polygeneration by a moving bed:

characteristics of products and energy efficiency analysis. Bioresour. Technol. 254, 130–138. https://doi.org/10.1016/j.biortech.2018.01.083.

Zhao, Y., Zhang, R., Liu, H., Li, M., Chen, T., Chen, D., Zou, X., Frost, R.L., 2019. Green preparation of magnetic biochar for the effective accumulation of Pb(II): Performance and mechanism. Chem. Eng. J. 375, 122011 https://doi.org/10.1016/j.cej.2019.122011.

Zhi, Y., Zhang, C., Hjorth, R., Baun, A., Duckworth, O.W., Call, D.F., Knappe, D.R.U., Jones, J.L., Grieger, K., 2020. Emerging lanthanum (III)-containing materials for phosphate removal from water: a review towards future developments. Environ. Int. 145, 106115 https://doi.org/10.1016/j.envint.2020.106115.